Acta of Bioengineering and Biomechanics
Vol. 3, No. 1, 2001

Biomechanical analysis of a new type of compressive splint used in carpal arthrodesis

ONDŘEJ JIROUŠEK

Institute of Theoretical and Applied Mechanics, Academy of Sciences of the Czech Republic, Prague.

JIŘÍ MÁCA

Czech Technical University, Faculty of Civil Engineering, Prague, Czech Republic.

JOSEF JÍRA

Czech Technical University, Faculty of Transportation Sciences, Prague, Czech Republic.

This paper presents a numerical analysis of the state of stress in a new type of splint used for carpal arthrodesis. Using the finite element method we evaluated the state of stress of the splint and the respective bones in two important load cases. Results of the numerical analysis were confirmed by photoelasticity test applied to the splint model. A qualitative comparison of different approaches to modelling short bones used in the finite element method is also made.

Key words: compressive splint, carpal arthrodesis, state of stress, short bone modelling

1. Introduction

Numerical analysis of the state of stress in the splint and the bones in carpal arthrodesis is carried out. The splint is a new type of compressive, dorsally concave splint taking on natural shape of the bone skeleton. It was developed in co-operation with the 2nd Medical Faculty of Charles University in Prague. The splint is applied to the second and third metacarpi and to the radius by means of cortical screws.

The main problem in carpal arthrodesis of wrist is the fixation of metacarpal region [4]. The classical AO method of stationary osteosynthesis and/or the application of a DC splint (figure 1) is associated with certain problems of how to fix this region. Also the effects of the position of splintage on the displacement of fractures are

known and studied [11]. *Regio dorsi manus* is a region, in which the bone skeleton is covered with a very thin layer of soft tissue only. In the distal part of the hand, we deal with more serious problem. In this region, the skin is separated from deeper structures by a thin layer of subcutaneous tissue only; moreover, the venous plexus and often also the extensor tendons rise to the surface in this region. In the case of classical AO splint, the skin at the dorsal part of the hand is greatly stretched and may hinder free movement of the extensors [10].

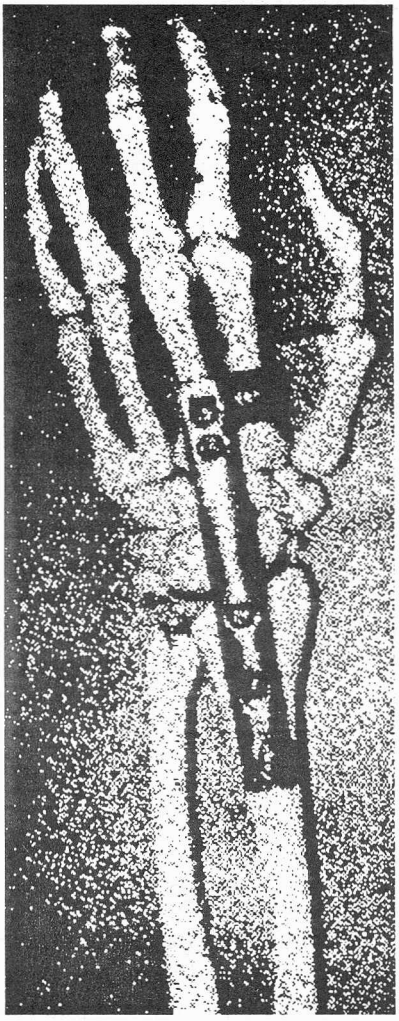

Fig. 1. Application of the splint to the model

To assure a sufficient three-point fixation, the splint must be shifted distally as much as possible which makes the straining of the soft tissues even worse. In the case of rheumatic patients, there is also the danger of skin ischemization. Moreover, the holes in the respective bones reduce substantially the strength of the diaphysis of the second and the third metacarpi.

It is for the aforementioned reasons that it became necessary to design a new implant, which would enable a three-point fixation by means of its distal end. The splint was designed in such a way as such to reduce the implant thickness to a minimum in order to prevent straining of the tissues of the dorsum. Another important reason for reducing the splint thickness is to minimise the amount of metal inserted into the region. Two implant variants appeared advantageous – one in the form of inverted L, the other (a T-shaped variant) enabling even a four-point fixation of the metacarpal region. Finally, the first variant was chosen, chiefly to reduce the application of metal material in the hazardous region. The short arm of the splint always points to the radial side and serves as the fixation of the second metacarpus. The distal part of the long arm is fastened to the third metacarpus with two screws. The splint's proximal end is fastened to the radius with three or four cortical screws.

Two oval openings in the long arm of splint fulfil another important task. Their margins are so formed as to enable self-compression after screw tightening. The application of the splint to the hand skeleton begins with the application of these screws. The autocompressive tightening of these screws produces pressure on the radial and metacarpal parts of the carpal joint shifting both lateral parts to the central part. The axial compression increases the stability of the osteosynthesis and improves

the contact of bone fragments. The thickness of splint material reaches 2.8 mm. This is the marginal value for the provision of the autocompressive openings. The stainless steel of the implant is known under the technical name of AKV ULTRA 2 Poldi CSN 17350. The strength of this generally recognised osteosynthesis material ranges from 880 to 1080 MPa. Because of a small splint thickness a soft tissue cover at the dorsal part of the hand may comply with low requirements, does not produce skin stretching, etc. The convex shape of the splint not only contributes to the bending strength of the implant but it also reduces significantly the tissue straining in the dorsal part of the hand, particularly in the metacarpal region.

The objective of the paper was to determine the state of stress of the splint and to reduce the splint thickness to a minimum, while preserving splint toughness to ensure good fixation of the metacarpal region. Another task was to establish the influence of the splint on the state of stress of the bones being connected. Generally, the implant bending stiffness was one of the key features examined, so we conducted some preliminary parametric studies in order to estimate the splint thickness. It should be stressed that most of an available literature reports on clinical trials, while this article is one of the first to address the biomechanical aspect of the problem [4], [5].

2. State of stress of the splint

The computations were based on the finite element method using the ANSYS 5.3 computational system. The experimental verification of the numerical analysis was carried out by the photoelastic method using a two-dimensional splint model. First, we computed numerically the stress field (figure 2) in the splint body by the FEM using the ANSYS 5.3 system [1]. We considered two states of load. Immediately after application the splint is subjected to compression caused by the screw tightening. However, this stress is negligibly small, as the bones in the metacarpal region are cut into small pieces left in situ, and we assumed modulus of elasticity of this bone filling very small. Apart from this the stress after splint application relaxes fast.

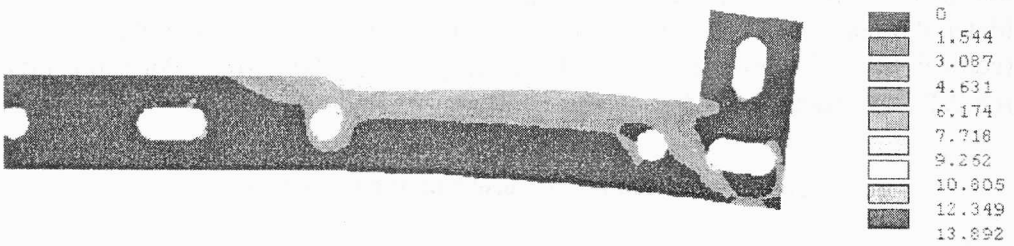

Fig. 2. Field of the first principal stresses in the splint body

The centre of gravity of the hand was ascertained 38 mm distally from the axis passing through the openings on the bases of the second and the third metacarpi using

simplified CAD model of the wrist with bone and flesh tissue density specified. In the first stage, we assumed only the dead load of the hand, which was determined as 10 N using the same CAD model. The first load acts in the radioulnar direction, the second one simulates palmar flexion in the pronation position of the hand and the carpus. The mathematical model consisted of 3108 isoparametric shell elements and 6555 nodal points. We used shell element which was determined by eight nodal points with six degrees of freedom at each. The load was acting in the nodal points of the openings. The maximum stress value σ_I in the first state of load (13.9 MPa) is low compared with the strength of the steel used (800 MPa). In terms of stress, the second state of load is more important when it is applied perpendicularly to the splint plane. The maximum stress value σ_I is 87.8 MPa.

3. Numerical analysis of short bone behaviour

The other task was to determine the state of stress in the respective bones. In the first part of this section, several approaches to bone modelling were compared. The bone is a nonhomogeneous anisotropic material consisting of two different materials: compact bone forming the outer bone surface (cortical bone) and the inner part of the bone filled with trabecular (or cancellous) bone. Longitudinally the bone consists of two parts. The central part, where the cortical bone layer is thicker, is called diaphysis. Toward the epiphyses the thickness of cortical bone decreases until it changes with no discontinuity into the cancellous bone.

One of the objectives of this project was to compare the individual approaches to simplified short-bone modelling. The comparison was based on a model of the second metacarpus subjected to a simple load. The cortical part of the metacarpus was modelled by means of shell elements of either constant or variable thickness and by brick elements. In another model of metacarpus, also the cancellous bone tissue was considered together with the cortical shell to verify the assumption that in the case of this type of loading the cancellous part of the bone could be neglected due to its far lower modulus of elasticity and that the modelling of the cortical shell only was sufficient. Material properties of the cortical and cancellous bones were taken from the literature (cortical bone: Young's modulus of elasticity E = 17000 MPa, Poisson's ratio $\mu = 0.26$; cancellous bone: E = 1600 MPa, $\mu = 0.29$ [3]).

3.1. Comparison of different metacarpus models

For the modelling purposes we selected the model of the second metacarpus, firmly constrained at the proximal end and loaded with a unite load at the distal end of material characteristics specified above. All models consisted of the same number of elements of identical shape. Higher-order elements, i.e. elements with intermediate nodes, were always used.

3.1.1. Brick elements

The first model analysed was that consisting of the cortical part of the bone only, modelled using brick elements with respect to the variable thickness of the cortical shell along the longitudinal axis. The geometric model of the bone was determined by sample measurements. Four characteristic cross-sections were measured and the thickness of the cortical bone was determined from X-ray photos. From the ANSYS element library a 20-node brick element was chosen.

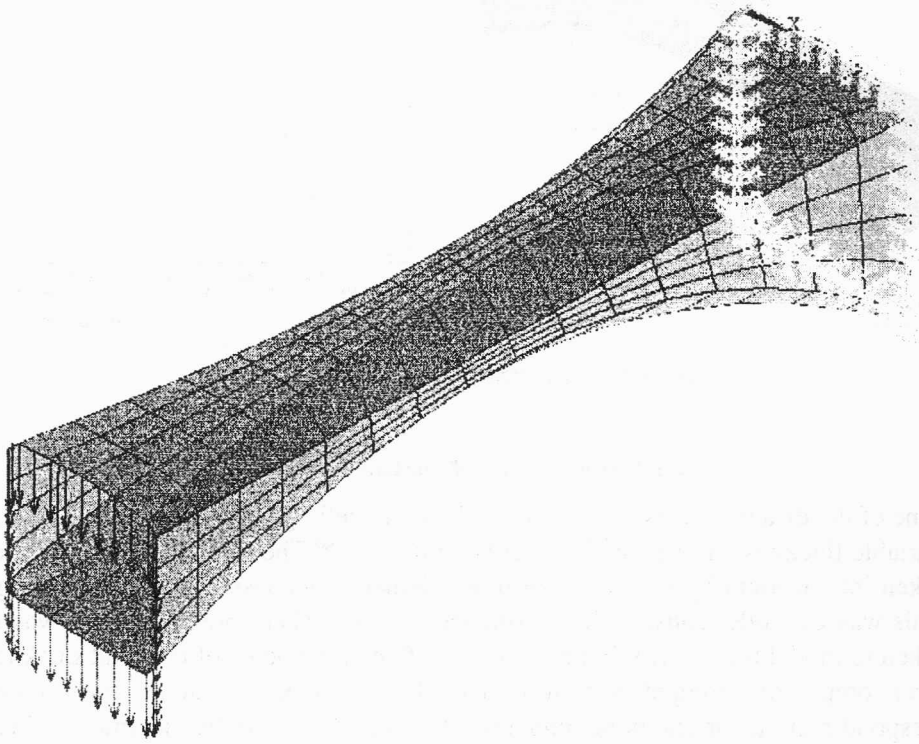

Fig. 3. Model of the third metacarpus

The number of elements, being the same for all other models, was 320. The way of load application and the constraint of the metacarpus modelled are shown in figure 3. In particular the maximum stress value, the stress distribution along the upper bone surface, the extreme stress magnitude, the maximum deformation and the vertical displacement of the free end were compared. Figure 4 shows the field of the principal stresses σ_1 as well as their distribution along the upper surface of metacarpus. Local stress concentration due to the effects of the forces applied takes place on the loaded end of the metacarpus. Further extreme values were found in the constrained end and in the place of cross-sectional area reduction. The maximum stress value of 4.9 MPa

was attained in the constraint. Another local maximum was in the place of cross-sectional area reduction. The value of the vertical displacement of the free end of this model reached 0.11 mm.

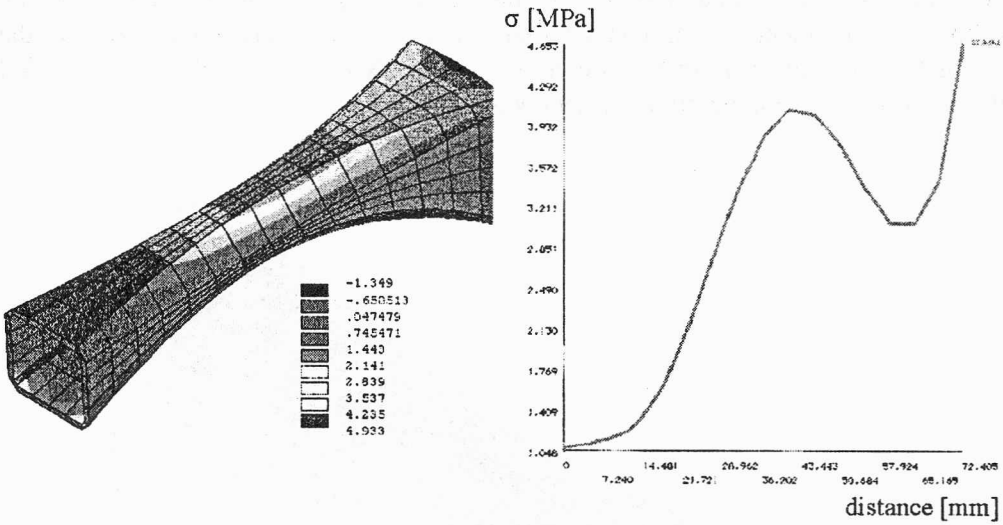

Fig. 4. Principal stresses protect σ_I (SOLID95)

3.1.2. Shell elements of constant thickness

One of the disadvantages of the cortical bone modelling using the shell elements is its variable thickness in the longitudinal bone direction. The thickness variability can be taken into account by the variation in an element thickness of individual "rings", but this way of model construction is time-consuming. Therefore an attempt was undertaken to model the cortical bone by means of shell elements of constant thickness. Several comparative computations were made for the thickness ranging from 0.5 mm (corresponding to a cortical bone thickness at the epiphysis) to the maximum value of 2 mm (in the centre of the diaphysis). The results were compared with the results of metacarpus analysis modelled by means of brick elements.

The best results were obtained when the average thickness determined on the basis of the longitudinal bone section was used. Numerical values of the results of the models with minimum, maximum and this comparative thickness were compared. The shortcoming of a bone modelling by means of shell elements is that it does not provide any reduction of flexural rigidity from the centre outwards. The stress peak occurs only in the place of the anatomical narrowing of the bone which, however, simultaneously coincides with the greatest cortical bone thickness, while the maximum stress values are expected in the constrained metacarpus end. If possible ways of bone stresses are considered, it is consequently advisable to take into account the variable cortical bone thickness in the computations.

3.1.3. Elements of variable thickness

It seems that modelling the cortical bone by means of shell elements of variable thickness is a better way. Thickness of the element between the cross-sections measured was assumed to change linearly. The change in element thickness was effected in every element ring.

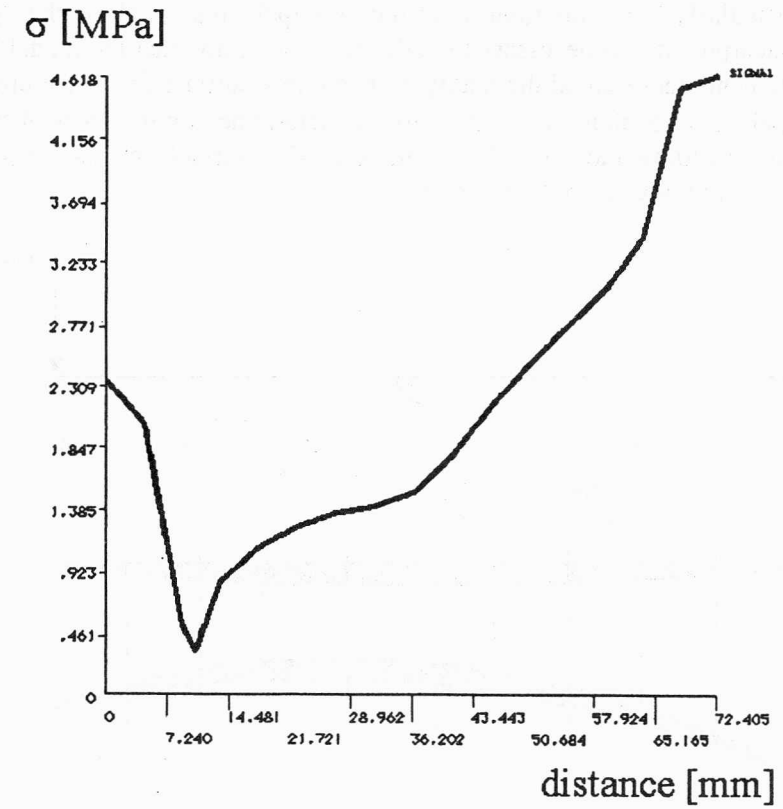

Fig. 5. Distribution of σ_I along the upper side of metacarpus – shell elements with variable thickness

The individual thicknesses were precisely obtained from 3D model. This variant approaches the solid element variant in size and position of extreme values. However, the distribution of the stresses σ_I along the upper surface of bone (figure 5) reveals that the central part of the bone is considerably stiffer compared with other parts and that there is no stress concentration in this place.

The best way to overcome this shortcoming was to establish the optimum thickness of the element in the central part of the bone by a number of approximations. We obtained the most promising results when the element thickness was reduced by 40% in its central part. The comparison of the results of the individual models was based in particular on the distribution of the principal stresses along the upper surface of meta-

carpus. In conclusion we can state that when modelling the cortical bone of short carpal ossicles using the shell elements of variable thickness it is advisable to reduce the flexural stiffness of the central part of the cortical bone.

3.1.4. Verification of the stress distribution

The results obtained revealed some indispensable differences between individual models, particularly in the distribution of the principal stress σ_1 along the upper surface of metacarpus. It was necessary to verify the assumption that the model based on the brick elements represented the reality best. For this purpose the distribution of the first principal stress σ_1 along the same path was determined on the basis of the distribution of the bending moment of a cantilever of a variable cross-section loaded similarly as the previous models (figure 6).

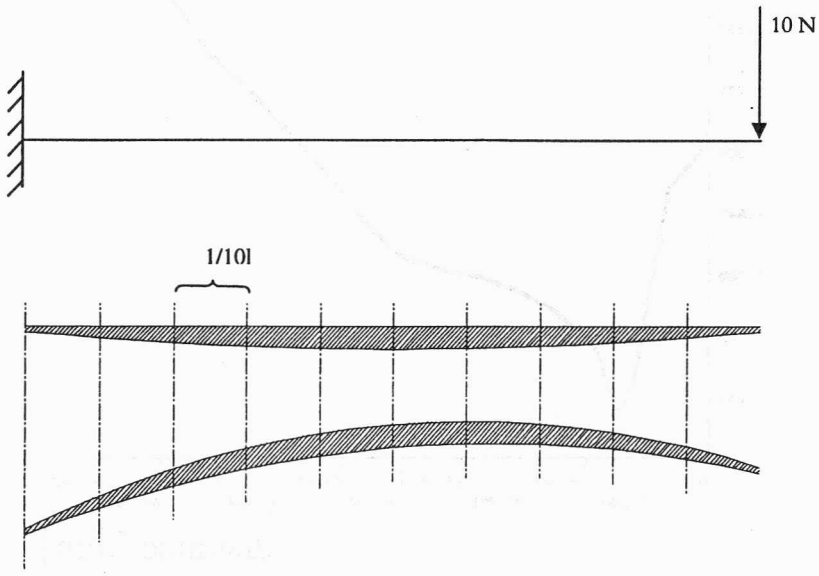

Fig. 6. Cantilever with variable cross-section section

The values of stresses were determined in ten characteristic points of the cantilever. The moment of inertia of each individual cross-section was determined on the basis of geometry data precisely obtained from the ANSYS system. The cross-sectional characteristics of individual cross-sections are shown in the table. The distribution of the stresses σ_x is very similar to the distribution in the case of the model with brick elements. The stress concentration occurs again both in the place of cross-sectional area reduction and at the constrained end. In conclusion, it is possible to state that modelling of cortical bone of short bones of human hand by means of brick elements gives better results than the same modelling with shell elements either of constant or variable thickness.

Table. Cross-sectional characteristics

Section	Area [mm^2]	I_x [mm^4]	M_x [N·mm]	W [mm^3]	σ_x [MPa]
1	26.61	726.83	0	120.00	0.00
2	41.67	789.2	72.4	146.64	0.49
3	48.34	657.69	144.8	135.91	1.07
4	50.49	522.61	217.2	117.39	1.85
5	51.04	440.99	289.6	104.03	2.78
6	52.18	429.94	362	101.66	3.56
7	55.28	512.99	434.4	114.87	3.78
8	60.28	750	506.8	149.76	3.38
9	64.30	1229.7	579.2	208.81	2.77
10	60.21	1917.8	651.6	268.67	2.43
11	35.94	1981.5	724	233.20	3.10

3.1.5. Some remarks about cancellous bone

In the preceding models the cancellous part of the bone was not taken into account due to far lower value of its modulus of elasticity. The purpose of the next comparative model was to establish the influence of the cancellous bone on the state of stress of the bone. The cancellous part of the bone was modelled by means of brick elements SOLID95.

The comparison was made using the same model of the third metacarpus with cortical shell modelled either by brick elements or by shell elements of variable thickness, including the stiffness compensation in the central part of the bone given in the preceding chapter. The results prove that there exists a certain positive influence of the cancellous bone on the stress distribution in the bone. However, incorporation of the cancellous bone into this type of loading does not have a significant influence on the stress distribution in the bone body. In our case, the difference in the stress distributions in these two models was less than 10%. If a certain type of loading produces maximum stresses in the epiphyses of short bone, it is advisable to incorporate into the analysis not only the cortical bone, but also the cancellous bone. This method of bone modelling, however, has one serious disadvantage. A large volume of spongy bone increases also the number of elements and, consequently, the computing time. In standard physiological situations, the loads applied to a bone usually do not produce the danger of failure at the bone end, but in its diaphysis. For these loads, therefore, the modelling of the cortical part of the bone only is sufficient.

4. State of stress of bones

The results presented earlier allow us to determine the state of stress of the whole system comprising the splint, the radius and both metacarpi. As a result of two com-

putations, the connected bones were modelled either by means of shell elements with variable thickness or by means of brick elements.

4.1. Shell elements

The bones were provided with appropriate openings of the diameter identical to the diameter of cortical screws used. The radius was firmly constrained at its proximal end. The load of a 10 N at a distance of 38 mm from the axis passing through the openings in the distal splint part (corresponded to the position of centre of gravity of

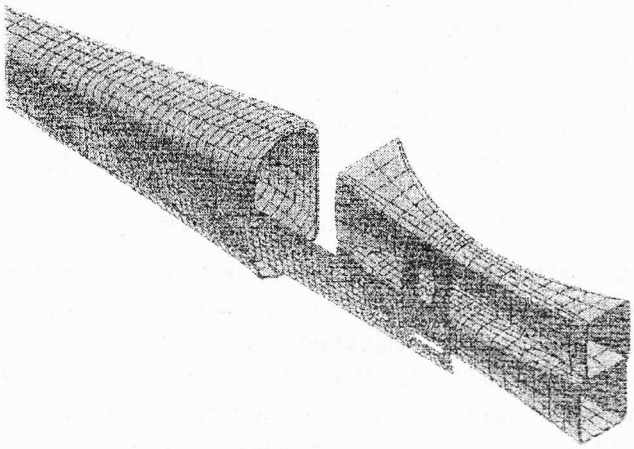

Fig. 7. Mathematical model

the hand) was distributed regularly among the two metacarpi and realised by nodal forces of corresponding magnitudes. The finite element model (figure 7) consisted of 4293 elements. The mathematical characteristics used for the cortical bone were identical to the preceding models.

4.1.1. Determination of the state of stress

Again, we considered two load states. The fields of principal stresses in the splint body in both load states corresponded to the respective states of stress obtained from the numerical analysis of the splint without considering the bones. The distribution of the stress σ_I along the upper splint edge is shown in figure 8.

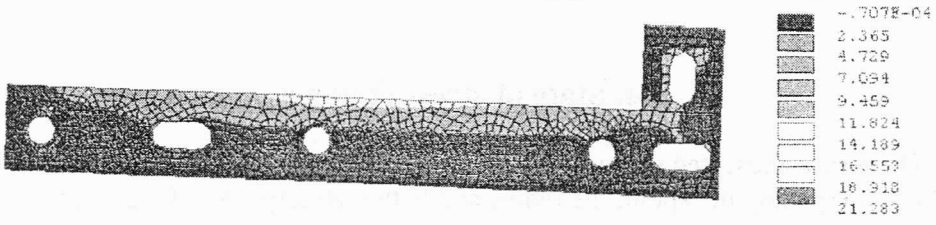

Fig. 8. Field of principal stress σ_I in the splint

The maximum value of stress in the cortical bone occurs in the second load state, which means that the load is applied perpendicularly to the splint plane (87.1 MPa). Stress concentration occurs at the distal part of the radius, near the most distal opening.

4.2. Brick elements

In order to compare the state of stress of the bones modelled by means of the brick elements, another model was constructed. In this model, both metacarpi and the radius were modelled using the 20-node solid element. The splint was modelled using the shell elements connected by rigid joints with the brick elements of the cortical bone in the location of openings. The total number of nodal points was 2592. The material characteristics were the same as in the preceding model.

4.2.1. Problems of mesh generation

As mentioned in the introduction to this chapter, the bones were modelled on the basis of four known cross-sections from which the model volume was generated by the interpolation of adequate surfaces. Four characteristic cross-sections were chosen in such a way as to capture the changes in the thickness of cortical layer. Mesh generation around the openings in the bones was the most serious problem. When we tried to use an automatic mesh generator (tetrahedral elements), the model of the second metacarpus consisted of more than 40,000 nodes which exceeded the limit of the university version of the ANSYS system.

Moreover, such a model would impose extensive requirements not only on the computing time, but also on the hard disk capacity (several gigabytes). Consequently, it was necessary to divide the bone volumes into adequate subvolumes of four or six surfaces and to use the non-degenerated brick elements. Four small volumes were created around each opening. The bones were then further divided into subvolumes in accordance with the thickness of the cortical layer. This dividing produced 112 subvolumes. When an automatic mesh generator was used, the variable thickness along the longitudinal bone axis posed the most crucial problem. The connection between the splint and the bones was modelled according to the previous model by means of rigid joints. Using the APDL (Ansys Parametric Design Language) we wrote a simple macro for automatic generation of these rigid joints. The proximal end of the radius was constrained, and both metacarpi were similarly loaded.

4.2.2. Determination of the state of stress

The global stiffness matrix of the problem approached 600 MB. First, we shall present the results of the first step of load. The field of the principal stresses σ_1 in the splint body corresponds with that in the previous model when shell elements of variable thickness are used.

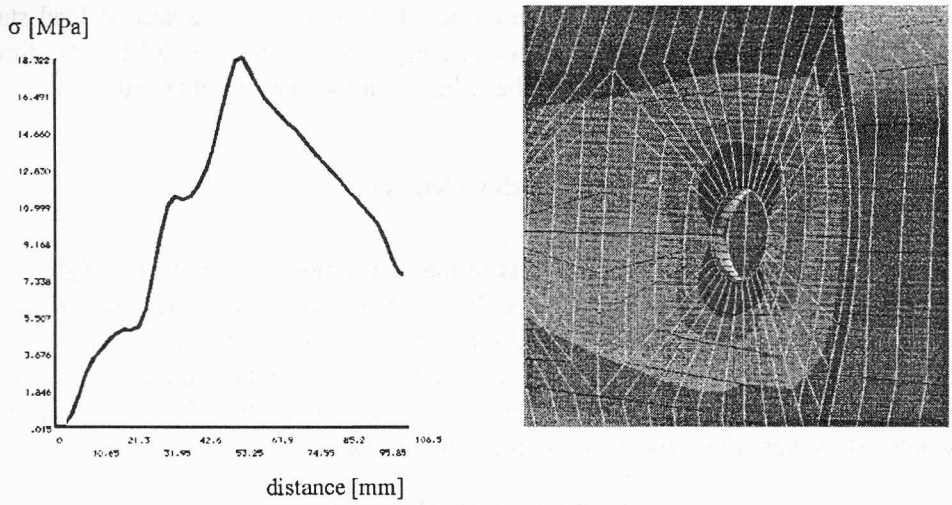

Fig. 9. Distribution of the principal stress σ_I along the upper split side and the stress field σ_{III} near the distal opening in the radius (the second state of load)

Figure 9 shows the distribution of the first principal stress along the upper edge of the splint. The stress concentration in the bones occurs in the place of the openings. The maximum value of the stress established in the first state if load reaches 34.5 MPa on the edge of the opening in the third metacarpus. The greatest stress concentration occurs in the second state of load in the vicinity of the third opening in the distal part of the radius as can be seen in the same picture. The maximum value of the principal stress σ_{III} is –77.6 MPa.

5. Experimental verification

In order to verify the results of the numerical analysis of the splint, a plane model of the splint was made of Perspex material on the scale of 2:1. The radius and both metacarpi were modelled by means of plane Plexiglas plates. The splint was applied by means of steel pins to the Plexiglas plates. The plate representing the radius was firmly fastened to the loading frame. The model was loaded by means of a lever mechanism. The end of the lever was loaded with a 7 kg weight. The material of the splint was assumed to be linear and we only did the qualitative comparison, therefore the load could be chosen arbitrarily.

5.1. State of stress of the specimen

Determination of the state of stress of the specimen described is based on the integration of the Lamé–Maxwell constants which are valid from the unloaded margin

towards the centre of the specimen. A photograph of isochromatic lines of the loaded model is shown in figure 10.

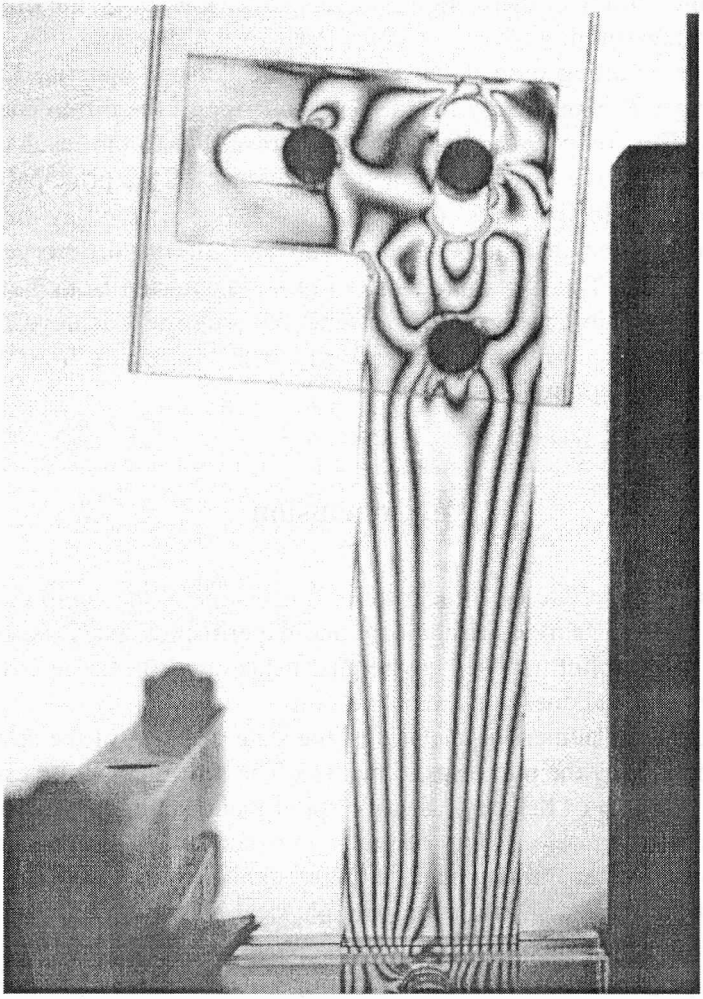

Fig. 10. Isochromatic lines of the loaded model

In order to determine the stress distribution from the isochromatic lines, one had to know the optical sensitivity of the material. The optical sensitivity of the specimen was obtained from a specimen of circular form. This specimen was loaded with symmetric load, and the diffraction values established by the compensation measurements for rising and dropping load were plotted in a diagram. The optical sensitivity of the material is given by the formula:

$$K = \frac{8P}{\pi d \Delta},$$

where P is the load applied, d is the diameter of a circular specimen and Δ is the diffraction value. The measured values were weighted by the least square method. In terms of the inaccuracy of diffraction readings under low loads, the diffraction value from the first measurement was not considered in the determination of the optical sensitivity. The resulting optical sensitivity of the Perspex material K is 26.2. The optical sensitivity K is necessary for the determination of the differences of the principal stresses. The comparison of experimental results with the results of numerical analysis is based on the distribution of the difference of the principal stresses. The distribution of the principal stress difference $\sigma_I - \sigma_{III}$ determined by the ANSYS system is presented. The maximum established value of the difference of principal stresses is 10.2 MPa. The maximum value of $\sigma_I - \sigma_{III}$ obtained from the experiment is 11.9 MPa. In conclusion, it is possible to state that the results achieved by the photoelastic measurements correspond satisfactorily with the results from the numerical analysis of the plane splint model.

6. Conclusion

It was possible to reduce the thickness of a new type of the compressive splint for carpal arthrodesis by using computational and experimental analyses. Because of its small thickness the splint imposes low requirements on a soft tissue cover at the dorsal part of the hand and does not stretch the skin.

The results of the numerical analysis of the state of stress of the splint were verified experimentally by the photoelastic method. The maximum stress established was far below the strength of the steel used for splint manufacture, however, in computations the effect of muscles was not taken into account. This problem should be considered in further examinations. The splint stabilises very well the bones during treatment, but the patient should avoid any physical activities. Another problem was the analysis of the short bone behaviour.

Several approaches to short bone modelling were compared by means of the finite element method and using the general-purpose package ANSYS 5.3. The results of the analysis of the splint–bone system have revealed that the stresses originating in the bone are low compared with the strength of the cortical bone. Stress concentration occurs only on the edges of the openings. Experimental results have confirmed the correctness of the derived theoretical model of the splint behaviour in carpal arthrodesis. Therefore, the finite element model can be used for the simulation of various load states of the splint during the treatment.

Acknowledgement: This investigation was supported by the Grant Agency of the Academy of Sciences of the Czech Republic (grant number A2071003) as well as by the Research Funds CEZ:J04/98:212600025 and CEZ:J04/98:210000003.

References

[1] *ANSYS User Manual*, Vol. I–IV, 1993.

[2] BOYES J.H., *Bunnel's Surgery of the Hand*, Philadelphia, J.B. Lippincot, 1964.

[3] FUNG Y. C., *Biomechanics. Mechanical Properties of Living Tissues*, Springer-Verlag, New York –Heidelberg–Berlin, 1981.

[4] JÍRA J., JÍROVÁ J., *Computational modelling of state of stress during hand treatment*, Computer Methods in Biomechanics and Biomedical Engineering – 2, Gordon and Breach Science Publishers, 1998, pp. 431–438.

[5] JÍROVÁ J., *Biomechanics of hand implants*, Applied mechanics in the Americas, Vol. 6, Proceedings of Sixth Pan-American Congress of Applied Mechanics, Rio de Janeiro, Brazil, January 1999, published by AAM and ABCM, pp. 35–38.

[6] JIROUŠEK O., *State of stress of the splint and the bones in carpal arthrodesis*, VII Bilateral Czech –German Symposium "Significance of Hybrid Method for Assessment of Reliability and Durability in Engineering Sciences", the Liblice Castle, 1999, pp. 33–36.

[7] KOZIN S. H., MICHLOVITZ S. L., *Traumatic arthritis and osteoarthritis of the wrist*, Journal of Hand Therapy, April–June 2000, Vol. (13), 2, pp. 124–135.

[8] MULLEN T. M., *Static progressive splint to increase wrist extension or flexion*, Journal of Hand Therapy, October–December 2000, Vol. (13), 4, pp. 313–315.

[9] PECH J., *Carpal Arthrodesis* (in Czech), Nakladatelství Alter, 1994.

[10] PECH J., SOSNA A., *Our method of arthrodesis of the wrist*, Acta Chirurgica Ortop. Traumatol. Czech, 1993, Vol. (60), 5, pp. 287–295.

[11] YANNI D., LIEPPINS P., LAURENCE M., *Fractures of the carpal scaphoid. A critical study of the standard splint*, Journal of Bone Joint Surgery, July 1991, Vol. (73), 4, pp. 600–609.